

# Cosmological parameters from Planck data in $SU(2)_{\text{CMB}}$ , their local $\Lambda\text{CDM}$ values, and the modified photon Boltzmann equation

Ralf Hofmann<sup>1,\*</sup>, Janning Meinert<sup>1,2</sup>, and Shyam Sunder Balaji<sup>1</sup>

<sup>1</sup>Institut für Theoretische Physik, Universität Heidelberg Philosophenweg 12, D-69120 Heidelberg, Germany

<sup>2</sup>Department of Physics, Bergische Universität Wuppertal, Gaußstraße 20, D-42119 Wuppertal, Germany

A Preprint 7 June 2022

## ABSTRACT

A review of the spatially flat cosmological model  $SU(2)_{\text{CMB}}$ , minimally induced by the postulate that the Cosmic Microwave Background (CMB) is subject to an  $SU(2)$  rather than a  $U(1)$  gauge principle, is given. Cosmological parameter values, which are determined from the Planck CMB power spectra at small angular scales, are compared to their values in spatially flat  $\Lambda\text{CDM}$  from both local and global extractions. As a global model  $SU(2)_{\text{CMB}}$  leans towards local  $\Lambda\text{CDM}$  cosmology and is in tension with some global  $\Lambda\text{CDM}$  parameter values. We present spectral antiscreening / screening effects in  $SU(2)_{\text{CMB}}$  radiance within the Rayleigh-Jeans regime in dependence on temperature and frequency. Such radiance anomalies can cause CMB large-angle anomalies. Therefore, it is pointed out how  $SU(2)_{\text{CMB}}$  modifies the Boltzmann equation for the perturbations of the photon phase space distribution at low redshift and why this requires to solve the  $\ell$ -hierarchy on a comoving momentum grid ( $q$ -grid) for all  $z$ .

**Key words:** Thermal photon gas; deconfining  $SU(2)$  Yang-Mills thermodynamics; thermal ground state; temperature-redshift relation; cosmological model; modified dark sector; Planck-scale axions; fuzzy dark matter; galaxies; galactic structure; HSC-Y1; SDSS; SH0es; H0licow; KiDS; DES; CLASS

## 1 INTRODUCTION

Our present age witnesses a promising change in paradigm on how to model and analyse the composition and dynamics of the Cosmos. This shift is concerned with a departure from perturbative towards nonperturbative approaches.

Within flat  $\Lambda\text{CDM}$  one example on the modelling side is that nonlinear clustering observables (e.g., the galaxy-halo connection model) on cosmologically small comoving length scales (a few to tens of  $h^{-1}\text{Mpc}$ ), which evolve out of adiabatic, Gaussian initial perturbations, not only are addressed by mild multiplicative deformations of their perturbatively evolved versions Sugiyama et al. (2021) but by nonperturbative, high-resolution N-body simulations Miyatake et al. (2021, 2020). In contrast to the former the latter method does not require an anchoring in high- $z$  observables, which rely on a specific cosmological model, is valid if scales are not too small Miyatake et al. (2020), and exhibits large signal-to-noise ratios in weak lensing signals Miyatake et al. (2021).

An example on the theoretical side is deconfining  $SU(2)$  Yang-Mills thermodynamics with an a priori estimate of the thermal ground state based on selfdual, topologically nontrivial gauge-field configurations Hofmann (2016). Relying on this result, a postulate on the CMB being subject to an  $SU(2)$  rather than a  $U(1)$  gauge principle can be made, henceforth referred to as  $SU(2)_{\text{CMB}}$ , with its Yang-Mills scale (or critical temperature  $T_c$  for the deconfining-preconfining transition) fixed by CMB radio-frequency observations Fixsen et al. (2011); Hofmann (2009).

The flat  $\Lambda\text{CDM}$  model is a minimal and successful framework to accommodate a wealth of cosmological data Riess et al. (1998); Perlmutter et al. (1999); Alam et al. (2017); Bennett et al. (2003). Throughout the last decade, however, tensions were uncovered in certain parameter values of this model when determined by data referring to local vs. global cosmology, see Abdalla et al. (2022) for a recent, comprehensive review. Most profoundly, there is a Hubble crisis. This is expressed by a  $\sim 5\sigma$  discrepancy be-

tween the value  $H_0 \sim 73.5 \text{ km s}^{-1} \text{ Mpc}^{-1}$  (errors ranging between 1 and  $2.5 \text{ km s}^{-1} \text{ Mpc}^{-1}$ ) as extracted from the Hubble diagram in local, flat  $\Lambda\text{CDM}$ , see e.g. Riess et al. (2021), using calibrated standard candles, or from strong-lensing time delays (cosmography, only astrophysics model dependence), see Wong et al. (2020), and  $H_0 \sim (67.27 \pm 0.60) \text{ km s}^{-1} \text{ Mpc}^{-1}$  fitted to CMB two-point power spectra by the Planck collaboration Aghanim et al. (2020) with similarly low values obtained from BAO (standard ruler) data Alam et al. (2017) assuming flat  $\Lambda\text{CDM}$  to be valid globally. Next, global fits of flat  $\Lambda\text{CDM}$  and BBN yield a baryon density which is by a factor  $\sim 3/2$  higher than the value observed by direct baryon census, see e.g. Aghanim et al. (2020); Kirkman et al. (2003) for the former and Shull et al. (2012); Johnson et al. (2019) for the latter claim. Moreover, within flat  $\Lambda\text{CDM}$  weak gravitational lensing effects persistently indicate a value of the clustering amplitude Miyatake et al. (2021); Abbott et al. (2022); Heymans et al. (2021) which relates to a value of  $\sigma_8$  being by 2-3  $\sigma$  lower compared to the value extracted from CMB observation Aghanim et al. (2020); Nunes & Vagnozzi (2021). Also, there is a mild tendency for an increase of  $\Omega_m$  (by a maximum significance of  $\sim 1\sigma$  in Miyatake et al. (2021)) compared to the CMB extraction in Aghanim et al. (2020). Finally, we point out a  $\sim 2\sigma$  tension in the redshift  $z_{\text{re}}$  for reionisation between direct observation using the Gunn-Peterson trough Becker et al. (2001) and the latest extraction from the Planck data Aghanim et al. (2020). In addition to these anomalies in flat  $\Lambda\text{CDM}$  parameter values, there are large-angle anomalies in the CMB, hinting at a dynamical breaking of statistical isotropy relevant to these angular scales Tegmark et al. (2003); Gordon et al. (2005); Copi et al. (2006); Hofmann (2013). These anomalies can be distinguished as follows: lack of large-angle CMB temperature correlation, hemispherical power asymmetry, octopole planarity and alignment with the quadrupole, point-parity anomaly, variation in cosmological parameters over the sky, and cold spot. For a comprehensive, very recent summary see Abdalla et al. (2022).

The purpose of the present paper is twofold. In the first half we explain the cosmological model implied by  $SU(2)_{\text{CMB}}$  and its fit to Planck data in Hahn et al. (2019), in particular focusing on

\* E-mail: R.Hofmann@ThPhys.Uni-Heidelberg.de

the dark-sector parametrisation and a physical realisation thereof proposed in [Meinert & Hofmann \(2021\)](#). Flat  $\Lambda$ CDM emerges at low redshifts in this model, and we compare the according parameter values with those of recent weak-lensing and galaxy clustering analyses, local Hubble-diagram fits, observations of the onset of the epoch of reionisation by the detection of the Gunn-Peterson trough in the spectra of distant quasars, and direct baryon censuses. This is confronted with the extraction of flat  $\Lambda$ CDM parameters in global cosmology probes (CMB and BAO). As a result, we see a tendency that  $\Omega_m$  is increased and  $\sigma_8$  decreased compared to these global fits. In particular, the latest results on weak-lensing galaxy-galaxy correlation using the HSC Y1 and SDSS data yield coinciding central values of these two parameters with those of the model in [Hahn et al. \(2019\)](#), albeit the significance of  $\Omega_m$ 's deviation only is  $1\sigma$ . Moreover, the model in [Hahn et al. \(2019\)](#) obtains values of other cosmological parameters which point towards the values extracted from local probes, most noticeably the value of  $H_0 \sim (74.24 \pm 1.46) \text{ km s}^{-1} \text{ Mpc}^{-1}$  deviates by less than  $1\sigma$  from that of [Riess et al. \(2021\)](#). The latter, in turn, deviates from global extractions in flat  $\Lambda$ CDM by more than  $5\sigma$ . In the second half of the paper we revisit the modification of the conventional Planck spectrum of blackbody radiance at low frequencies and temperatures with the intention to eventually implement this spectral anomaly into a particular CMB Boltzmann solver – CLASS [Ma & Bertschinger \(1995\)](#); [Lesgourgues \(2011\)](#); [Blas et al. \(2011\)](#). We suppose [Szopa & Hofmann \(2008\)](#); [Ludescher & Hofmann \(2009\)](#); [Hofmann \(2013\)](#) that a proper implementation of the according comoving energy-momentum relation in such a code conveys some of the above mentioned large-angle anomalies [Tegmark et al. \(2003\)](#); [Copi et al. \(2006\)](#) even though the projection onto  $C_\ell$ 's assumes statistical isotropy. Presently, we face technical problems in the implementation, however. This concerns the introduction of a grid in comoving momentum  $q$  for the photon Boltzmann hierarchy. Therefore, no results on the low- $\ell$  CMB angular power spectra are presented here<sup>1</sup>. Hoping that experts in the CMB modelling community can be interested in overcoming these problems in a reasonable amount of time, desirably in collaboration with the present authors, we provide the required comoving photon dispersion law in  $\text{SU}(2)_{\text{CMB}}$ .

This paper is organised as follows. In Sec. 2 we review the minimal, spatially flat cosmological model  $\text{SU}(2)_{\text{CMB}}$ , as it was employed in [Hahn et al. \(2019\)](#) in fits to 2015 Planck data. We also discuss dark-sector physics, based on ultralight Planck-scale axion species [Meinert & Hofmann \(2021\)](#), which the minimal dark sector of  $\text{SU}(2)_{\text{CMB}}$  in [Hahn et al. \(2019\)](#) may be mimicking. Cosmological parameter values extracted in [Hahn et al. \(2019\)](#) are compared with global and recent local extractions within flat  $\Lambda$ CDM or by cosmography to point out a tendency of  $\text{SU}(2)_{\text{CMB}}$  as a global model leaning towards local, flat  $\Lambda$ CDM. Sec. 3 first provides a brief review of large-angle anomalies in the CMB, based on analyses of the two satellite mission WMAP and Planck. The radiatively induced antiscreening/screening effects in the Rayleigh-Jeans regime, which are described by the screening function  $G$  for the thermal  $\text{SU}(2)_{\text{CMB}}$  photon, could explain the CMB large-angle anomalies, see [Ludescher & Hofmann \(2009\)](#); [Hofmann \(2013\)](#). Therefore, we review this blackbody anomaly of spectra radiance both as a function of temperature and frequency. It is pointed out that the maximal deviation between  $\text{U}(1)$  and  $\text{SU}(2)_{\text{CMB}}$  radiances is constantly feeble at temperatures considerably larger than  $T_c = T_0 = 2.725 \text{ K}$ , rendering its detection at high tempera-

tures, say  $T = 300 \text{ K}$ , experimentally challenging. Next, we discuss the effects of screening function  $G$  on the Boltzmann equation for the cosmological evolution of linear perturbations of photon phase-space distribution in conformal Newtonian gauge. Since low-redshift (low- $z$ ) photons suffer antiscreening/screening a nontrivial comoving energy-momentum relation persists, exhibiting a dependence on conformal time  $\tau$ . Moreover, a match between high- $z$  and low- $z$  evolution needs to be made when solving the Boltzmann hierarchy on a comoving momentum grid ( $q$ -grid) for *all*  $\tau$ , including active Thomson scattering. Finally, we point out which modules of the Boltzmann code CLASS are affected by the modified cosmological model  $\text{SU}(2)_{\text{CMB}}$  to simultaneously address the CMB power spectra at high- $\ell$  for cosmological parameter extraction and at low- $\ell$  to mitigate the discrepancy of TT power seen in [Hahn et al. \(2019\)](#). Such a lowering of TT power would be a smoking gun for the breaking of statistical isotropy at low redshift mediated by  $\text{SU}(2)_{\text{CMB}}$ .

## 2 PRESENT STATUS OF $\text{SU}(2)_{\text{CMB}}$

### 2.1 $T$ - $z$ relation and other implications for the cosmological model

The change due to  $\text{SU}(2)_{\text{CMB}}$  in spatially flat FLRW cosmology, which, as a background model, appreciably starts deforming  $\Lambda$ CDM at redshifts well within the dark ages, is induced by a modified CMB temperature ( $T$ ) - redshift ( $z$ ) relation. For the reader's convenience we repeat here the arguments put forward in [Hahn et al. \(2019\)](#) how this modification comes about and what it implies.

In an (energy conserving) FLRW universe one demands

$$\frac{d\rho_{\text{YM}}}{da} = -\frac{3}{a} (\rho_{\text{YM}} + P_{\text{YM}}), \quad (1)$$

where  $\rho_{\text{YM}}$  and  $P_{\text{YM}}$  denote energy density and pressure, respectively, in the deconfining phase of  $\text{SU}(2)$  Yang-Mills thermodynamics (subscript  $\text{YM}$ ), and  $a$  refers to the cosmological scale factor, normalised to  $a(T_0) = 1$ , where  $T_c = T_0 = 2.725 \text{ K}$  indicates the present baseline temperature of the CMB [Mather et al. \(1990\)](#), interpreted as the critical temperature  $T_c$  for the deconfining-preconfining phase transition in [Hofmann \(2009\)](#). The solution of Eq. (1) can be recast as

$$a \equiv \frac{1}{z+1} = \exp\left(-\frac{1}{3} \log\left(\frac{s_{\text{YM}}(T)}{s_{\text{YM}}(T_0)}\right)\right). \quad (2)$$

Here the entropy density  $s_{\text{YM}}$  is given as

$$s_{\text{YM}} \equiv \frac{\rho_{\text{YM}} + P_{\text{YM}}}{T} \quad (3)$$

which shows that the a priori estimates of the thermal ground-state contributions to pressure and energy density do not contribute to Eq. (2). For large temperatures,  $T \gg T_0$ , Eq. (2) can be simplified [Hahn & Hofmann \(2018\)](#) as

$$\frac{T(z)}{T_0} = (1/4)^{1/3} (z+1) \approx 0.63 (z+1). \quad (4)$$

The basis  $1/4$  is the ratio between the number  $n_P$  of relativistic degrees of freedom in constituting the gauge-field excitations of the plasma at  $T_0$  ( $n_P = 2$ ) and for  $T \gg T_0$  ( $n_P = 8$ ). For temperatures  $T$  not much higher than  $T_0$  linearity in the  $T$ - $z$  relation is violated by the Yang-Mills scale  $\Lambda$  (related to  $T_0$  by  $\Lambda = 2\pi T_0/13.87$  [Hofmann \(2016\)](#)) breaking conformal invariance. Therefore, we define the multiplicative deviation  $S(z)$  from linear scaling at any given temperature  $T$  in the deconfining phase as

$$S(z) = \left( \frac{\rho_{\text{YM}}(z=0) + P_{\text{YM}}(z=0)}{\rho_{\text{YM}}(z) + P_{\text{YM}}(z)} \frac{T^4(z)}{T_0^4} \right)^{1/3}. \quad (5)$$

<sup>1</sup> Note that the information residing in the  $C_\ell$ 's is just a projection of the isotropy breaking effect since their computation assumes statistical isotropy. In [Tegmark et al. \(2003\)](#); [Copi et al. \(2006\)](#); [Vielva \(2010\)](#) for example, statistics are considered which measure the breaking of statistical isotropy without such a projection.

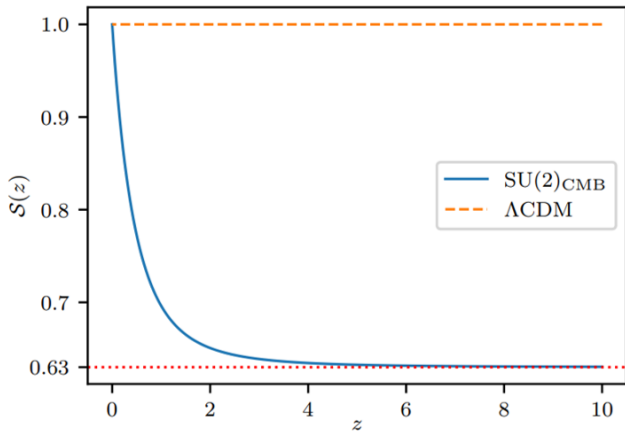


Figure 1: Plot of function  $S(z)$  of Eq. (5), defined as a (multiplicative) deviation from the linear  $T$ - $z$  relation of Eq. (4). The curvature in  $S(z)$  at low  $z$  indicates the breaking of conformal invariance in the deconfining  $SU(2)$  Yang-Mills plasma for  $T \sim T_0$  with a rapid approach towards  $(1/4)^{1/3} \approx 0.63$  as  $z$  increases. Figure adapted from [Hahn et al. \(2019\)](#).

As a result, the  $T$ - $z$  relation assumes the generally valid form

$$\frac{T(z)}{T_0} = S(z)(z+1) \quad (T \geq T_0). \quad (6)$$

Fig. 1 depicts function  $S(z)$ . For the conformally invariant Yang-Mills gas and for  $T \gg T_0$ , when all eight gauge modes are nearly massless<sup>2</sup>, the  $z$  dependence of the deconfining Yang-Mills energy density  $\rho_{\text{YM}}$  is implied by Eq. (4) to be

$$\rho_{\text{YM}}(z) = 4 \left(\frac{1}{4}\right)^{4/3} \rho_{\gamma}(z) = \left(\frac{1}{4}\right)^{1/3} \rho_{\gamma}(z) \quad (z \gg 1). \quad (7)$$

Here,  $\rho_{\gamma}$  denotes the energy density of a thermal photon gas, using the  $U(1)$   $T$ - $z$  relation  $T = T_0(z+1)$ . Again, for low temperatures conformal invariance is broken, and Eq. (7) needs to be modified accordingly, see [Hahn et al. \(2019\)](#). For the  $z$  dependence of the energy density of massless neutrinos one has for  $T \gg T_0$

$$\Omega_{\nu}(z) = \frac{7}{8} N_{\text{eff}} \left(\frac{16}{23}\right)^{4/3} \Omega_{\text{YM},\gamma}(z). \quad (8)$$

In Eq. (8) a modified factor for the conversion of neutrino to CMB temperature occurs because of additional relativistic degrees of freedom during  $e^+e^-$  annihilation [Hofmann \(2015\)](#),  $\Omega_{\text{YM},\gamma}(z)$  refers to the photon part of the density parameter in deconfining  $SU(2)_{\text{CMB}}$  thermodynamics (screening/antiscreening effects, off-Cartan fluctuations, and thermal ground-state contribution excluded), and  $N_{\text{eff}}$  is the effective number of massless neutrino flavours. As in [Hahn et al. \(2019\)](#) we set  $N_{\text{eff}}$  equal to its 2015 Planck value [Ade et al. \(2016\)](#):  $N_{\text{eff}} = 3.046$ .

The postulate  $SU(2)_{\text{CMB}}$  affects the comoving sound horizon  $r_s(z)$ , whose value at recombination (baryon drag) is the anchoring scale for the analysis of large-scale structure based on BAO, not only directly via the Hubble parameter  $H(z)$  but also indirectly via the sound velocity  $c_s$  of the baryon-Yang-Mills plasma conventionally modelled in terms of baryons interacting via photons. In general,  $r_s(z)$  is given as

$$r_s(z) \equiv \int_z^{\infty} dz' \frac{c_s(z')}{H(z')}, \quad (9)$$

<sup>2</sup> Two polarisations for the massless mode, three polarisations for each of the two massive modes.

where the sound velocity is represented by

$$c_s(z) \equiv \frac{1}{\sqrt{3(1+R(z))}}. \quad (10)$$

In what follows the subscript  $L$  refers to the quantity computed in  $\Lambda$ CDM. Specifically, the ratio  $R_L$  relates to entropy densities  $s_L$  or energy densities  $\rho_L$  of baryons (b) and photons ( $\gamma$ ) as

$$R_L \equiv \frac{s_{L,b}(z)}{s_{L,\gamma}(z)} = \frac{3 \rho_{L,b}(z)}{4 \rho_{L,\gamma}(z)} \quad (z \gg 1). \quad (11)$$

The generalisation of Eq. (11) to the baryon-Yang-Mills plasma replaces  $s_{L,\gamma}(z)$  or  $\rho_{L,\gamma}(z)$  by  $s_{\text{YM}}(z)$  or  $\rho_{\text{YM}}(z)$ , respectively, and  $s_{L,b}$  or  $\rho_{L,b}(z)$  by  $s_{\text{YM},b}$  or  $\rho_{\text{YM},b}(z)$ , respectively, to define  $R_{\text{YM}}$ , see [Hahn et al. \(2019\)](#).

For the epoch of recombination the postulate  $SU(2)_{\text{CMB}}$  predicts a significantly higher redshift than  $\Lambda$ CDM does. Namely, equating the temperature of both models at  $T \gg T_0$ , using Eq. (4) for  $SU(2)_{\text{CMB}}$  and  $T/T_0 = z+1$  for  $\Lambda$ CDM, we arrive at

$$z_L = \left(\frac{1}{4}\right)^{1/3} z_{\text{YM}}. \quad (12)$$

In particular, this yields

$$z_{\text{YM,rec}} = 1730, \quad (13)$$

based on  $z_{L,\text{rec}} = 1090$  [Ade et al. \(2016\)](#); [Aghanim et al. \(2020\)](#). Repeating the argument of [Hahn et al. \(2019\)](#), we now infer from Eq. (13) a dramatic reduction of the matter density parameter  $\Omega_{\text{YM},m,0}$  during the epoch of recombination in  $SU(2)_{\text{CMB}}$  compared to  $\Lambda$ CDM. For this purpose it is entirely sufficient to describe recombination in terms of thermodynamics (Saha approximation). The Thomson scattering rate  $\Gamma$  then is a function of the recombination temperature  $T_{\text{rec}}$  only:  $\Gamma = \Gamma(T_{\text{rec}})$ . Note that  $T_{\text{rec}}$  is independent of any cosmological model as long as thermodynamics prevails. Moreover, the Hubble parameter  $H$  depends on  $T_{\text{rec}}$  via  $z_{\text{rec}}$ :  $H(z_{\text{rec}}) = H(z(T_{\text{rec}}))$ . The additional assumption, that  $H$  is matter dominated during recombination turns out to be selfconsistent, see [Hahn et al. \(2019\)](#). Eliminating  $\Gamma$  from the decoupling conditions in both models,  $H_{\text{YM}}(z_{\text{YM,rec}}) = \Gamma(T_{\text{rec}}) = H_L(z_{L,\text{rec}})$ , we thus conclude that

$$\Omega_{L,m,0} \approx 4 \Omega_{\text{YM},m,0}. \quad (14)$$

The most economic way for the modified cosmological model to simultaneously obey the postulate  $SU(2)_{\text{CMB}}$  globally and mimic  $\Lambda$ CDM at low redshifts<sup>3</sup> is the instantaneous emergence of dark matter (edm) from dark energy at some redshift  $z_p < z_{\text{YM,rec}}$ . From now on we set  $z \equiv z_{\text{YM}}$ . Therefore, the following density parameter for the dark sector (ds) was proposed in [Hahn et al. \(2019\)](#):

$$\Omega_{\text{ds}}(z) = \Omega_{\Lambda} + \Omega_{\text{pdm},0}(z+1)^3 + \Omega_{\text{edm},0} \begin{cases} (z+1)^3, & (z < z_p) \\ (z_p+1)^3, & (z \geq z_p) \end{cases}. \quad (15)$$

In Eq. (15) today's density parameters for dark energy and dark matter are denoted by  $\Omega_{\Lambda}$  and  $\Omega_{\text{pdm},0} + \Omega_{\text{edm},0} \equiv \Omega_{\text{cdm},0}$ , respectively,  $\Omega_{\text{pdm},0}$  refers to primordial dark matter for all  $z$ , and  $\Omega_{\text{edm},0}$  associates with dark matter emergent from dark energy at  $z_p$ . In the following a brief discussion of the physics, potentially responsible for the dark-sector model in Eq. (15), is given following reference [Meinert & Hofmann \(2021\)](#). There the dark sector starts out at the Big Bang with four species of dark energy three of which have undergone transitions into dark matter in the past; one species yet

<sup>3</sup> The success of  $\Lambda$ CDM as a low- $z$  model is suggested by the agreement of its parameter values when extracted from purely local and different cosmology probes, see [Abdalla et al. \(2022\)](#).

is to face such a transition and therefore plays the role of a cosmological constant at present. The theoretical underpinning of such a dark-sector model is the invocation of the axial anomaly by SU(2) Yang-Mills theories, subject to a universal Planckian Peccei-Quinn scale *Giacosa et al. (2008)*. Three out of four theories presently are in confining phases with their Yang-Mills scales relating to the masses of charged leptons. Such a link to particle physics is based on the assertion that lepton doublets are emergent phenomena in pure SU(2) Yang-Mills theories *Hofmann (2018); Hofmann & Grandou (2022)*. The associated *axion* particles receive their masses  $m_a$  via the axial anomaly *Adler & Bardeen (1969); Adler (1969); Bell & Jackiw (1969); Fujikawa (1979, 1980)* invoked by topological charges residing in the ground states of these Yang-Mills theories and are ultralight. With a universal Planckian Peccei-Quinn scale axion masses  $m_a$  thus scale like the squares of charged lepton masses  $m$ , e.g.  $m_{a,\mu}/m_{a,e} = m_\mu^2/m_e^2$  *Meinert & Hofmann (2021)*.

A depercolation transition from a homogeneous, superhorizon sized axion condensate (dark energy) towards a gas of non-relativistic lumps (cold dark matter) of fuzzy dark matter (condensate core / soliton plus Navarro-Frenk-White halo) *Sin (1994); Ji & Sin (1994); Matos & Guzman (2000); Schive et al. (2014); Niemeyer (2020)* occurs when the Hubble radius  $r_H$  matches the Bohr radius  $r_B$  modulo a phenomenologically determined, multiplicative constant  $\alpha_e \sim 55,500$ , compare with *Meinert & Hofmann (2021)*. For the axion particle associated with the electron this depercolation transition is parameterised in Eq. (15) to occur at  $z_p = z_{p,e} = 53$ . The two other depercolation transitions, associated with the muon and the tau, are found to occur at  $z_{p,\mu} = 40,000$  and  $z_{p,\tau} = 685,000$  in *Meinert & Hofmann (2021)*, respectively. Because the Hubble radius at  $\tau$ -lump depercolation is  $r_H(z_{p,\tau} = 685,000) \sim 1.36 \times 10^{-6}$  Mpc this corresponds to a lower comoving cutoff scale of 0.93 Mpc for the linear density contrast generated by adiabatic curvature perturbations. For  $\mu$ -lump depercolation we have  $r_H(z_{p,\mu} = 40,000) \sim 3.74 \times 10^{-4}$  Mpc, corresponding to a comoving cutoff scale of 14.94 Mpc. These two cutoff scales are well inside the nonlinear regime *Miyatake et al. (2021)*. For e-lump depercolation  $r_H(z_{p,e} = 53) \sim 16.48$  Mpc is obtained, associated with a comoving cutoff scale of 873 Mpc. Therefore, the assumption made in *Meinert & Hofmann (2021)* that density perturbations in the e-lump gas are triggered by those of the  $\tau$ -lump and  $\mu$ -lump gases is consistent for comoving scales up to 873 Mpc. Beyond this scale e-lump density perturbations are seeded by adiabatic curvature perturbations upon their horizon entry.

## 2.2 Cosmological parameters: SU(2)<sub>CMB</sub> vs. local and global observations in $\Lambda$ CDM

The spatially flat, global cosmological model, minimally implied by SU(2)<sub>CMB</sub> as outlined in Sec. 2.1, and flat  $\Lambda$ CDM, considered as a globally valid cosmological model, produce the parameter values in the table below when fitted to 2015 Planck data *Hahn et al. (2019)*, for the corresponding TT power spectrum see appendix A. For completeness we also quote the values of flat  $\Lambda$ CDM fitted to 2018 Planck data *Aghanim et al. (2020)*:

As the table indicates, there are statistically significant deviations between flat SU(2)<sub>CMB</sub> and flat  $\Lambda$ CDM, most noticeably in  $H_0$ . This  $\sim 4.6$  to  $4.7 \sigma$  discrepancy is comparable to the one extracted from the Hubble diagram in *local* flat  $\Lambda$ CDM, see e.g. *Riess et al. (2021)*, using calibrated standard candles, or from strong-lensing time delays (cosmography, only astrophysics model dependent extraction of  $H_0$ ), see *Wong et al. (2020)*. On the other hand, fits of flat  $\Lambda$ CDM to BAO (standard ruler) and 2015 Planck data *Alam et al. (2017)* yield a value of  $H_0$  which is close to the fit of flat  $\Lambda$ CDM to the 2015 and 2018 Planck data alone:  $(67.6 \pm 0.5) \text{ km s}^{-1} \text{ Mpc}^{-1}$  vs.  $(67.51 \pm 0.64) \text{ km s}^{-1} \text{ Mpc}^{-1}$

Parameter	SU(2) <sub>CMB</sub>	$\Lambda$ CDM (2015)	$\Lambda$ CDM (2018)
$\omega_{b,0}$ .....	$0.0173 \pm 0.0002$	$0.02226 \pm 0.00016$	$0.02237 \pm 0.00015$
$\omega_{\text{pdm},0}$ .....	$0.113 \pm 0.002$	–	–
$\omega_{\text{cdm},0}$ .....	$0.0771 \pm 0.0012$	–	–
$100 \theta_s$ .....	$1.0418 \pm 0.0022$	$1.0408 \pm 0.00032$	$1.04092 \pm 0.00031$
$\tau_{\text{re}}$ .....	$0.02632 \pm 0.00218$	$0.063 \pm 0.014$	$0.0544 \pm 0.0073$
$\ln(10^{10} A_s)$ .....	$2.858 \pm 0.009$	$3.059 \pm 0.025$	$3.044 \pm 0.014$
$n_s$ .....	$0.7261 \pm 0.0058$	$0.9653 \pm 0.0048$	$0.9649 \pm 0.0042$
$z_p$ .....	$52.88 \pm 4.06$	–	–
$H_0 / \text{km s}^{-1} \text{ Mpc}^{-1}$ .....	$74.24 \pm 1.46$	$67.51 \pm 0.64$	$67.36 \pm 0.54$
$z_{\text{re}}$ .....	$6.23^{+0.41}_{-0.42}$	$8.5^{+1.4}_{-1.2}$	$7.67 \pm 0.73$
$z_*$ .....	$1715.19 \pm 0.19$	$1090.00 \pm 0.29$	$1089.92 \pm 0.25$
$z_d$ .....	$1640.87 \pm 0.27$	$1059.62 \pm 0.31$	$1059.94 \pm 0.30$
$\omega_{\text{cdm},0}$ .....	$0.1901 \pm 0.0023$	$0.1193 \pm 0.0014$	$0.1200 \pm 0.0012$
$\Omega_\Lambda$ .....	$0.616 \pm 0.006$	$0.6879 \pm 0.0087$	$0.6847 \pm 0.0073$
$\Omega_{m,0}$ .....	$0.384 \pm 0.006$	$0.3121 \pm 0.0087$	$0.3153 \pm 0.0073$
$\sigma_8$ .....	$0.709 \pm 0.020$	$0.8150 \pm 0.0087$	$0.8111 \pm 0.0060$
$S_8 \equiv \sigma_8 \sqrt{\Omega_{m,0}/0.3}$ .....	$0.802 \pm 0.029$	$0.8313 \pm 0.0176$	$0.8315 \pm 0.0137$
$\text{Age} / \text{Gyr}$ .....	$11.91 \pm 0.10$	$13.807 \pm 0.026$	$13.797 \pm 0.023$

Table 1: Best-fit cosmological parameters of flat SU(2)<sub>CMB</sub> to the data in *Ade et al. (2016)* (1st column) as well as flat  $\Lambda$ CDM model to the data in *Ade et al. (2016)*, employing the TT,TE,EE+lowP+lensing likelihoods (2nd column) and to the data in *Aghanim et al. (2020)*, employing the TT,TE,EE+lowE+lensing likelihoods (3rd column). For SU(2)<sub>CMB</sub> the HiLLiPOP+lowTEB+lensing likelihood is used as defined in *Aghanim et al. (2016)* (lowP and lowTEB are pixel-based likelihoods). The upper section of the table quotes free parameter values, the lower section states the values of derived parameters. Errors correspond to 68% confidence levels.

(Planck 2015) and  $(67.36 \pm 0.54) \text{ km s}^{-1} \text{ Mpc}^{-1}$  (Planck 2018), respectively. All cosmological parameters are  $\sim 1 \sigma$  consistent in flat  $\Lambda$ CDM (2015) and flat  $\Lambda$ CDM (2018).

Let us now discuss baryon density  $\omega_{b,0}$ . Global fits of flat  $\Lambda$ CDM to the Planck data and BBN yield a baryon density which is by about a factor  $\sim 3/2$  higher than the value observed by direct, local census, see e.g. *Ade et al. (2016); Aghanim et al. (2020); Kirkman et al. (2003)* for the former and *Shull et al. (2012); Johnson et al. (2019)* for the latter claim. The significance of this deviation is about  $2 \sigma$ . The same tendency of such a discrepant value of  $\omega_{b,0}$  is seen in the table when comparing flat SU(2)<sub>CMB</sub> and flat  $\Lambda$ CDM, albeit at a higher significance.

Next, in  $\Lambda$ CDM weak gravitational lensing effects persistently indicate a value of the clustering amplitude *Miyatake et al. (2021); Abbott et al. (2022); Heymans et al. (2021)*, characterised by  $\sigma_8 = 0.718^{+0.044}_{-0.031}$  in *Miyatake et al. (2021)*, which is by  $2\text{--}3 \sigma$  lower compared to its value extracted from CMB observation, see table and *Ade et al. (2016); Aghanim et al. (2020)*. As the table indicates, in SU(2)<sub>CMB</sub> the same tendency occurs, subject to a higher significance of  $5.3 \sigma$ . Also, there is a mild tendency for an increase of  $\Omega_m$  in local observations (by a maximum significance of  $\sim 1 \sigma$  in *Miyatake et al. (2021)*) compared to the CMB extraction in *Ade et al. (2016); Aghanim et al. (2020)*. Such a tendency is also seen in the table, albeit now with a significance of  $7.5 \sigma$ .

Finally, there is a  $\sim 2 \sigma$  tension in the redshift  $z_{\text{re}}$  for reionisation between direct observation using the Gunn-Peterson trough *Becker et al. (2001)* and extraction of  $z_{\text{re}} = 7.67 \pm 0.73$  from the 2018 Planck data *Aghanim et al. (2020)*. For the 2015 Planck data,  $z_{\text{re}} = 8.5^{+1.4}_{-1.2}$  this tension is again at  $\sim 2 \sigma$ . From the table we see that the tension between flat SU(2)<sub>CMB</sub> and flat  $\Lambda$ CDM is  $1.6 \sigma$  (2015 Planck data) and  $2 \sigma$  (2018 Planck data).

It is conspicuous that the *global* flat model SU(2)<sub>CMB</sub> yields key cosmological parameter values which agree better with those of *local* flat  $\Lambda$ CDM extractions rather than those of *global* flat  $\Lambda$ CDM fitted to the same Planck data. Notice the unusually low value of the spectral index  $n_s$  of adiabatic curvature perturbations in SU(2)<sub>CMB</sub>, indicating a red-tilted spectrum. This may turn out to be an artefact of velocity divergence being suppressed on smaller

scales due to late-time axion-condensate depercolation (e-lumps) but a modelling of the transition through an instantaneous transmission of this perturbation from the primordial gas ( $\mu$ -lumps and  $\tau$ -lumps), see [Hahn et al. \(2019\)](#). That is, in reality the primordial spectrum may well be scale invariant but is fitted to be red-tilted due to missing velocity divergence on smaller scales. To gain more confidence in such an interpretation a thorough modelling of the depercolation transition in the framework of fuzzy dark matter (Poisson-Schrödinger system) is required, see e.g. [Schive et al. \(2014\)](#).

### 3 CMB AT LARGE ANGLES

#### 3.1 Observational situation

As exhibited in Sec. 2.2, the global cosmological model flat  $\Lambda$ CDM deviates in some key parameter values from both local flat  $\Lambda$ CDM and the global flat model  $SU(2)_{\text{CMB}}$  (fitted to Planck data and determined by angular scales associated with  $l > 50$  [Abdalla et al. \(2022\)](#); [Hahn et al. \(2019\)](#)). In addition, there are inadequacies at large angular scales, see, e.g. [Hinshaw et al. \(1996\)](#); [Tegmark et al. \(2003\)](#); [Copi et al. \(2007, 2015b\)](#), for missing power in the TT correlation on angular scales larger than  $60^\circ$  and the breaking of statistical isotropy expressed by low- $\ell$  multipole alignment in the map of CMB temperature fluctuations [Gordon et al. \(2005\)](#); [Copi et al. \(2006, 2011\)](#); [Hofmann \(2013\)](#). More specifically, based on the analysis of the two satellite missions WMAP and Planck, CMB large-angle anomalies fall into one of the following categories: lack of large-angle CMB temperature correlation (sketched above), hemispherical (dipolar) power and variance asymmetries, e.g. [Eriksen et al. \(2004\)](#); [Ade et al. \(2016\)](#); [Akrami et al. \(2020\)](#), octopole planarity and alignment with the quadrupole, e.g. [de Oliveira-Costa et al. \(2004\)](#); [Copi et al. \(2015a\)](#); [Notari & Quartin \(2015\)](#); [Schwarz et al. \(2016\)](#), point-parity anomaly, e.g. [Kim & Naselsky \(2010\)](#); [Aluri & Jain \(2012\)](#); [Gruppuso et al. \(2018\)](#), variation in cosmological parameters over the sky, e.g. [Fosalba & Gaztañaga \(2021\)](#); [Yeung & Chu \(2022\)](#), and cold spot, e.g. [Vielva et al. \(2004\)](#); [Cruz et al. \(2010\)](#); [Akrami et al. \(2020\)](#).

There are many attempts at explaining the CMB large-angle anomalies in the literature, ranging from a nontrivial topology of the Universe over an unusually large matter void invoking the integrated Sachs-Wolfe effect to features in the spectra of initial perturbations, see [Abdalla et al. \(2022\)](#) for a recent compilation of these proposals. Here instead we focus on a dynamical, late-time breaking of statistical isotropy which peaks at redshift  $z \sim 1$  and is induced by screened / antiscreened photon propagation in the framework of  $SU(2)_{\text{CMB}}$  [Hofmann \(2013\)](#). This effect is expected to reduce the low- $\ell$  excess in the TT power spectrum of [Hahn & Hofmann \(2017\)](#), see appendix A.

#### 3.2 Modified $SU(2)_{\text{CMB}}$ dispersion law and CMB Boltzmann solvers

##### 3.2.1 Modified photon radiance in $SU(2)_{\text{CMB}}$

As explained in [Schwarz et al. \(2007a\)](#); [Hofmann \(2007\)](#), the modified black-body spectral intensity  $I_{\text{SU}(2)}(\nu)$  of the  $SU(2)$  theory is obtained from that of the conventional  $U(1)$  theory as follows

$$I_{\text{SU}(2)}(\nu) = I_{\text{U}(1)}(\nu) \times \left(1 - \frac{G(\nu)}{\nu^2}\right) \theta(\nu - \nu^*), \quad (16)$$

where the characteristic cutoff-frequency  $\nu^*$  is defined implicitly through

$$|\vec{p}|(\nu^*) = \sqrt{(2\pi\nu^*)^2 - G} = 0, \quad (17)$$

and  $\theta(x)$  denotes the Heaviside function. It was shown in [Falquez et al. \(2010\)](#) that

$$\nu^*(T) \propto T^{-1/2}, \quad (T \gg T_c). \quad (18)$$

In SI units one has

$$I_{\text{U}(1)}(\nu) \equiv \frac{2h}{c^2} \nu^3 n_B \left(\frac{h\nu}{k_B T}\right), \quad (19)$$

where  $k_B$  is Boltzmann's constant,  $h$  is Planck's quantum of action,  $c$  denotes the speed of light in vacuum, and  $n_B(x) \equiv 1/(e^x - 1)$ . For the massless mode propagating into the spatial 3-direction,  $\vec{p}||e_3$ , and resorting back to natural units,  $c = k_B = \hbar = 1$ , the screening function  $G(\nu)$  is computed in cylindrical coordinates and reads [Schwarz et al. \(2007b\)](#)

$$\frac{G}{T^2} = \int d\xi \int d\rho e^2 \lambda^{-3} \left(-4 + \frac{\rho^2}{4e^2}\right) \rho \frac{n_B\left(\frac{2\pi\lambda^{-3/2}\sqrt{\rho^2 + \xi^2 + 4e^2}}{\sqrt{\rho^2 + \xi^2 + 4e^2}}\right)}{\sqrt{\rho^2 + \xi^2 + 4e^2}}, \quad (20)$$

where  $\lambda \equiv 13.87 T/T_c$  ( $T_c$  the critical temperature for the deconfining-preconfining phase transition), and  $e$  denotes the effective gauge coupling  $e \geq \sqrt{8}\pi$ . The support of the integration in Eq. (20) is determined from the demand that  $\rho$  and  $\xi$  satisfy one or both of the two following conditions

$$\left| \frac{G}{T^2} \frac{\lambda^3}{(2\pi)^2} \pm \frac{\lambda^{3/2}}{\pi} \left( \sqrt{X^2 + \frac{G}{T^2}} \sqrt{\rho^2 + \xi^2 + 4e^2} - X\xi \right) + 4e^2 \right| \leq 1, \quad (21)$$

where  $X = X(T, \nu) \equiv |\vec{p}|/T = \sqrt{(2\pi\nu)^2 - G}/T$ . For the  $SU(2)$  radiance one obtains [Falquez et al. \(2010\)](#)

$$L_{\text{SU}(2)}(T, \nu) = L_{\text{U}(1)} \times \left(1 - \frac{G}{(2\pi\nu)^2}\right) \theta(\nu - \nu^*), \quad (22)$$

and specifically for  $SU(2)_{\text{CMB}}$  one has  $T_c = T_0 = 2.725$  K [Fixsen et al. \(2011\)](#); [Hofmann \(2009\)](#). In Fig. 2 the temperature dependence of spectral black-body radiance in the range from 0 – 30 K is shown for five different frequencies in case of  $SU(2)_{\text{CMB}}$  and the conventional  $U(1)$  theory.

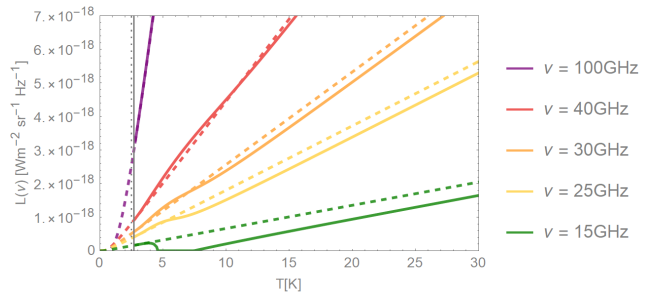


Figure 2:  $SU(2)$  Yang-Mills thermodynamics exhibits three phases [Hofmann \(2016\)](#): the confining phase below  $T_H \sim 0.9 T_c$  (the Hagedorn temperature  $T_H$  indicated by the vertical grey dotted line), the preconfining phase for  $T_H \leq T \leq T_c$  ( $T_c$  indicated by the vertical grey line), and the deconfining phase for  $T \geq T_c$ . In  $SU(2)_{\text{CMB}}$  one has  $T_c = T_0 = 2.725$  K. SI units of radiance  $L(\nu)$  are  $\text{W m}^{-2} \text{sr}^{-1} \text{Hz}^{-1}$ . The  $U(1)$  Rayleigh-Jeans radiances are given in dashed lines for  $\nu = 15$  GHz (green), 25 GHz (yellow), 30 GHz (orange), 40 GHz (red), and 100 GHz (purple) while solid lines depict the associated radiances in  $SU(2)_{\text{CMB}}$ .

Notice the gap at the lowest frequency of 15 GHz and the shifted linear dependence (pseudo Rayleigh-Jeans) to the right of this gap due to screening in  $SU(2)_{\text{CMB}}$ . With increasing frequencies there is antiscreening at low temperature, which transitions

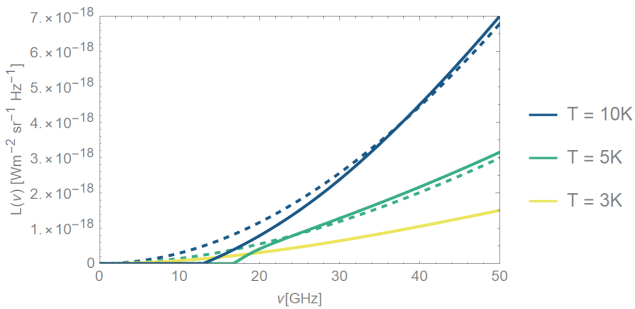


Figure 3: The  $SU(2)_{\text{CMB}}$  and the  $U(1)$  black-body spectral radiances are shown for  $T = 3$  K (yellow), 5 K (green), 10 K (blue) in solid and dashed lines, respectively. The spectral gap is widest at  $\sim 2 \times T_c \approx 5$  K. The spectral regime, where  $U(1)$  radiance is larger / smaller than  $SU(2)_{\text{CMB}}$  radiance, exhibits screening / antiscreening.

into screening at higher temperatures. Both temperature regimes, screening and antiscreening, approach the  $U(1)$  radiance rapidly as frequency increases. Fig. 3 depicts the frequency dependence of spectral black-body radiance from 0 to 50 GHz for three different temperatures. It can be seen from the spectra that the deviation  $\Delta L(\nu) \equiv |L_{U(1)}(\nu) - L_{SU(2)_{\text{CMB}}}(\nu)|$  is maximal at  $\nu = \nu^*$  where  $\Delta L(\nu) = L_{U(1)}(\nu)$ . This is true for all temperatures. Since  $L_{U(1)}(\nu) \propto \nu^2 T$  in the Rayleigh-Jeans regime and using Eq. (18), we conclude that

$$\Delta L(\nu^*) = 4.85 \times 10^{-19} \text{ W m}^{-2} \text{ sr}^{-1} \text{ Hz}^{-1}, \quad (T \gg T_c), \quad (23)$$

and in particular at room temperature. The feableness of such a small, maximal deviation between  $U(1)$  and  $SU(2)_{\text{CMB}}$  radiances renders the detection of the spectral anomaly at temperatures  $T \gg T_c$  an experimentally challenging task.

### 3.2.2 Boltzmann equation for linear perturbations of photon phase-space distribution

The low-frequency, low-temperature modifications of the thermal photon dispersion law in  $SU(2)_{\text{CMB}}$  discussed in Sec. 3.2.1 imply technical difficulties in the treatment of the Boltzmann hierarchy for the perturbations  $F_\gamma(\vec{k}, \hat{n}, q, \tau)$  and  $G_\gamma(\vec{k}, \hat{n}, q, \tau)$  of the photon phase-space distribution in CMB codes such as CLASS Lesgourgues (2011); Lesgourgues & Tram (2011). Here  $\hat{n} \equiv \vec{q}/q$ . These complications arise when evolving the latter, in comoving  $\vec{k}$ -space and at some comoving-momentum modulus  $q$ , through the low- $z$  (or large- $\tau$ ) regime Ma & Bertschinger (1995). More precisely, the low- $z$ , collisionless Boltzmann equation needs to maintain the  $q$ -dependence in the perturbations  $F_\gamma(\vec{k}, \hat{n}, q, \tau)$  and  $G_\gamma(\vec{k}, \hat{n}, q, \tau)$  because the ratio  $q/\epsilon$  ( $\epsilon$  the comoving energy, see Eq. (26) below) depends on conformal time  $\tau$ . Here we define the perturbations (sum and difference of perturbations associated with the two independent linear polarisation states)  $F_\gamma$  and  $G_\gamma$  through the perturbed phase-space distribution  $f$  as

$$f_\gamma(\vec{k}, \hat{n}, q, \tau) \equiv f_0(q) [1 + F_\gamma(\vec{k}, \hat{n}, q, \tau) + G_\gamma(\vec{k}, \hat{n}, q, \tau)], \quad (24)$$

where

$$f_0 = f_0(\epsilon) = \frac{1}{4\pi^3} \frac{1}{e^{\epsilon(q,a)/T_0} - 1}. \quad (25)$$

In Eq. (25)  $T_0$  is today's CMB temperature, and  $a$  denotes the cosmological scale factor with  $a(\tau_0) = 1$  where  $\tau_0$  refers to the present conformal time. In the case of thermalised photons in  $SU(2)_{\text{CMB}}$ , a

modified comoving energy-momentum dispersion law applies<sup>4</sup> Ma & Bertschinger (1995); Hofmann (2016) as

$$\epsilon(q, a) = \sqrt{q^2 + a^2 G(q, a)} = \sqrt{q^2 + \frac{G(q, z)}{(z+1)^2}} = \epsilon(q, z), \quad (26)$$

where  $G$  denotes the transverse screening function, discussed in Sec. 3.2.1 and given in Eqs. (20), (21), but now understood as a function of comoving momentum modulus  $q$  and scale factor  $a$  (or redshift  $z = 1/a - 1$ ) instead of  $X$  and  $T$ . We convert  $\frac{G}{T^2}(X, T)$  of Eq. (20) to  $G(q, z)$  by appealing to  $X = q(z+1)/T(z)$  and  $T(z)/T_0 = \mathcal{S}(z)(z+1)$ , see Eq. (6).

From Fig. 4 and Eq. (26) we infer that for increasing  $z$  one rapidly runs into the regime of the  $U(1)$  dispersion law,  $\epsilon = q$ . In particular, the  $U(1)$  dispersion law applies prior to and through recombination.

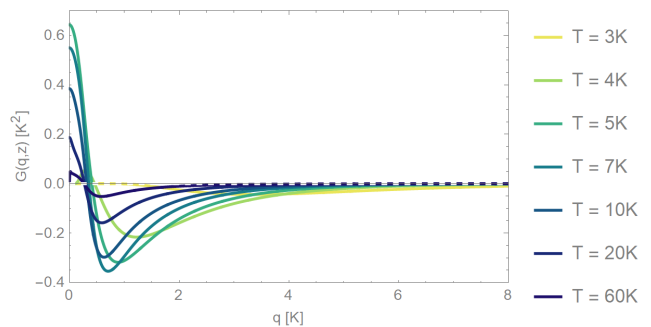


Figure 4: Screening function  $G(q, z)$  as a function of comoving momentum modulus  $q$  and for the following temperature / redshift values: 3 K ( $z = 0.29$ , yellow), 4 K ( $z = 1.16$ , light green), 5 K ( $z = 1.85$ , green), 7 K ( $z = 3.07$ , petrol), 10 K ( $z = 4.83$ , blue), 20 K ( $z = 10.66$ , dark blue), 60 K ( $z = 33.96$ , darkest blue). The white-dashed line depicts the  $U(1)$  situation  $G = 0$ .

In conformal Newtonian gauge, the linear perturbation  $\Psi(\vec{k}, \hat{n}, q, \tau) = F_\gamma(\vec{k}, \hat{n}, q, \tau) + G_\gamma(\vec{k}, \hat{n}, q, \tau)$  evolves according to the Boltzmann equation Ma & Bertschinger (1995)

$$\frac{\partial \Psi}{\partial \tau} + i \frac{q}{\epsilon} (\vec{k} \cdot \hat{n}) \Psi + \frac{d \ln f_0}{d \ln q} \left[ \phi - i \frac{\epsilon}{q} (\vec{k} \cdot \hat{n}) \psi \right] = \frac{1}{f_0} \left( \frac{\partial f}{\partial \tau} \right)_C, \quad (27)$$

where  $\phi$  and  $\psi$  are the gravitational potentials, and the right-hand side is the collision term. This term is only relevant prior to and through recombination and depends on  $F_\gamma(\vec{k}, \hat{n}, q, \tau)$  and  $G_\gamma(\vec{k}, \hat{n}, q, \tau)$  separately Ma & Bertschinger (1995). The expansion of  $F_\gamma(\vec{k}, \hat{n}, q, \tau)$  and  $G_\gamma(\vec{k}, \hat{n}, q, \tau)$  into Legendre polynomials  $P_\ell(\hat{k} \cdot \hat{n})$  ( $\ell = 0, 1, 2, \dots$ ) yields coefficients  $F_{\gamma, \ell}(\vec{k}, q, \tau)$  and  $G_{\gamma, \ell}(\vec{k}, q, \tau)$  which evolve in  $\tau$  (or  $z$ ) according to a Boltzmann hierarchy Ma & Bertschinger (1995). To perform a match of high- $z$  and low- $z$  (and therefore large-angle) downward evolutions at some appropriate, intermediate value  $z_{\text{match}}$  we notice that the need to retain the  $q$ -dependence in  $F_{\gamma, \ell}(\vec{k}, q, \tau)$  and  $G_{\gamma, \ell}(\vec{k}, q, \tau)$  at low  $z$  (not integrating it out) also requires to keep it at high  $z$  where anti-screening / screening effects of  $SU(2)_{\text{CMB}}$  can safely be neglected. Therefore, the Boltzmann hierarchy needs to be solved on a  $q$ -grid for all  $z$ . In Fig. 5 the  $z$ -evolution of the factor  $q/\epsilon$ , which induces this complication, is shown for low values of  $z$ .

<sup>4</sup> Even though the dependences of  $\epsilon(q, a)$  and  $G(q, a)$  on scale factor  $a$  and redshift  $z$  are different, we abuse notation by writing  $\epsilon(q, z)$  and  $G(q, z)$ .

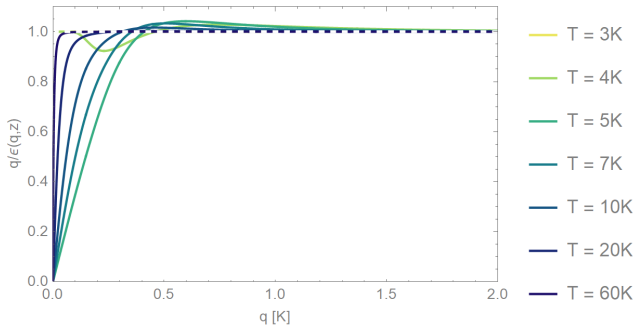


Figure 5: Shown is  $q/\epsilon(q, z)$  as a function of comoving momentum  $q$  and for the following temperature / redshift values: 3 K ( $z = 0.29$ , yellow), 5 K ( $z = 1.85$ , green), 7 K ( $z = 3.07$ , petrol), 10 K ( $z = 4.83$ , blue), 20 K ( $z = 10.66$ , dark blue), 60 K ( $z = 33.96$ , darkest blue). The  $U(1)$  behaviour  $q/\epsilon \equiv 1$  largely coincides with the behaviours at 3 K and 60 K and is shown in terms of a white-dashed line.

### 3.2.3 Structure of CLASS

Having (i) reviewed the main features of  $SU(2)_{\text{CMB}}$  as a cosmological model, see [Hahn et al. \(2019\)](#), and (ii) considered the CMB at large angular scales within deconfining  $SU(2)$  Yang-Mills thermodynamics, see [Ludescher & Hofmann \(2009\)](#); [Hofmann \(2013\)](#), we may now discuss what it takes to quantitatively confront  $SU(2)_{\text{CMB}}$  with the observed large-angle anomalies discussed in Sec. 3.1.

Several CMB Boltzmann codes are available such as CMBFAST [Seljak & Zaldarriaga \(1996\)](#), CMBEASY [Doran \(2005\)](#), CAMB [Lewis et al. \(2000\)](#), and CLASS [Lesgourgues \(2011\)](#). Here we choose to discuss CLASS due to its flexibility, speed, and good documentation which also has motivated its use in [Hahn et al. \(2019\)](#).

CLASS is written in pure C and includes the following modules: *input.c*, *background.c*, *thermodynamics.c*, *perturbations.c*, *primordial.c*, *nonlinear.c*, *transfer.c*, *spectra.c*, *lensing.c*, and *output.c*. Each of these modules perform specific tasks and feed their outputs into the subsequent module along the aforementioned order. The following modifications were implemented in [Hahn et al. \(2019\)](#):

(i) A module called *nonconventional.c* was added which computes the thermodynamical quantities  $\rho_{\text{YM}}$  (energy density),  $P_{\text{YM}}$  (pressure), and the scaling function  $\mathcal{S}(z)$  of Eqs. (5) and (6) in  $SU(2)_{\text{CMB}}$ .

(ii) The module *input.c* contains all input and precision parameters. Additional cosmological parameters in  $SU(2)_{\text{CMB}}$  such as  $z_p$ ,  $\Omega_{\text{edm},0}$  and the new conversion between the neutrino temperature  $T_\nu$  and the CMB temperature  $T$ , see Eq. (8), are introduced here.

(iii) The module *background.c* solves the Friedmann equation and stores other quantities such as the energy densities of individual species ( $\rho_i$ ), the critical density ( $\rho_c$ ), the Hubble parameter  $H$ , and conformal time  $\tau$ . Within this module, the new cosmological model is implemented according to Sec. 2.1. Also, the ratio  $R_{\text{YM}} \equiv \frac{s_b(z)}{s_{\text{YM}}(z)} = \frac{3}{4} \frac{\rho_b(z)}{\rho_{\text{YM}}(z)}$ , see Eq. (11) and text following it, is defined here.

(iv) The module *thermodynamics.c* evolves the baryon-photon plasma, relying on the modified sound speed  $c_s(z) \equiv 1/(3(1+R_{\text{YM}}(z)))$ , and stores quantities such as the ionisation fraction  $\chi_e$  as well as recombination and reionisation redshifts. The modified  $T-z$  relationship for  $SU(2)_{\text{CMB}}$  in Eq. (6) is implemented within this module.

(v) The module *perturbations.c* solves the perturbations evolution for each specified particle species and gravity. This module also includes the Euler equation for the emergent dark matter component [Hahn et al. \(2019\)](#).

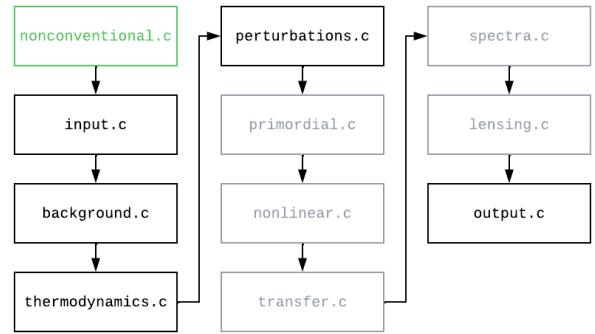


Figure 6: Modules of CLASS. The module *nonconventional.c* was introduced in [Hahn et al. \(2019\)](#) into the backbone of CLASS. The modules in black contain  $SU(2)_{\text{CMB}}$  modifications whereas the modules in gray are untouched.

(vi) The *output.c* module is extended to include the new  $SU(2)_{\text{CMB}}$  parameters.

All other modules, namely *primordial.c*, *nonlinear.c*, *transfer.c*, *spectra.c*, and *lensing.c* are not directly affected by  $SU(2)_{\text{CMB}}$ . Fig. 6 provides an overview on CLASS modules, how they depend on one another, and which modules are modified / added in [Hahn et al. \(2019\)](#) due to  $SU(2)_{\text{CMB}}$ . To address large-angle anomalies via a modification in the hierarchy for perturbations of the photon phase-space distribution, as discussed in Sec. 3.2.2, we foresee the following changes in the  $SU(2)_{\text{CMB}}$  modified version of CLASS:

(A) We are required to set up a function in *class.c* which calls the screening function  $G(q, z(\tau))$  for a given comoving momentum  $q$  and redshift  $z$  (and thus conformal time  $\tau$ ) from precomputed tables.

(B) In the *perturbations.c* module, the evolution of the perturbations of the photon phase-space distribution needs to be performed on a  $q$ -grid along an  $\ell$ -hierarchy (similar to the non-cold dark matter species description in [Lesgourgues & Tram \(2011\)](#)). This also requires the introduction of functions  $\epsilon$  (Eq. (26)) and  $q/\epsilon$  as well as the corresponding modification of  $\frac{d \ln f_0}{d \ln q}$  in Eq. (27).

The bottleneck is the implementation of the  $q$ -grid in the Boltzmann hierarchy for  $F_{\gamma,\ell}$  and  $G_{\gamma,\ell}$  which also involves the collision terms that are active prior to and throughout recombination (high- $z$  case). Moreover, a matching<sup>5</sup> at some intermediate  $z_{\text{match}}$  with  $1 \ll z_{\text{match}} \ll z_*$  of high- $z$  and low- $z$  evolutions needs to be implemented in *perturbations.c* on the  $q$ -grid such that power spectra do not depend on the choice of  $z_{\text{match}}$ .

It is hoped that a group with good experience in the implementation of the hierarchy for massive neutrinos in CLASS may be interested in pursuing the above mentioned code modifications, desirably in collaboration with the present authors.

## 4 SUMMARY AND OUTLOOK

In the present paper we have reviewed the cosmological model  $SU(2)_{\text{CMB}}$  which assumes that the CMB is subject to deconfining  $SU(2)$  Yang-Mills thermodynamics and a spatially flat Universe. This model coincides with flat  $\Lambda$ CDM locally. However, due to a modified temperature ( $T$ ) - redshift ( $z$ ) relation  $SU(2)_{\text{CMB}}$  deviates strongly from flat  $\Lambda$ CDM at high  $z$  with profound implications for the dark-sector physics. Cosmological parameter values, which are not affected by low- $z$  physics or the low- $\ell$  multipoles, were extracted

<sup>5</sup> Matching at  $z_{\text{match}}$  means that for  $z \geq z_{\text{match}}$  we set  $G \equiv 0$  in the Boltzmann hierarchy while  $G$  is taken from a precomputed table for  $z < z_{\text{match}}$ .

in [Hahn et al. \(2019\)](#) by fits to 2015 Planck power spectra. The corresponding model then yields an excess of low- $\ell$  power in TT which we address in the second part of the present paper in terms of photon screening / antiscreening effects at low  $z$ . Here, we confirm that there is indeed no influence of these effects on cosmological parameter fitting. We have compared the according parameter values of  $SU(2)_{\text{CMB}}$  with extractions from cosmologically local and global data within flat  $\Lambda\text{CDM}$  or within a cosmographic context. As a result, we see a tendency of  $SU(2)_{\text{CMB}}$  as a global model to lean towards locally extracted cosmological parameter values of  $H_0$ ,  $z_{\text{re}}$ ,  $\omega_b$ ,  $\sigma_8$ , and  $\Omega_m$ .

The low- $z$  spectral radiance antiscreening / screening anomalies in the Rayleigh-Jeans regime of deconfining  $SU(2)_{\text{CMB}}$  thermodynamics were not considered in [Hahn et al. \(2019\)](#) but are expected to relate to the large-angle anomalies of the CMB [Ludescher & Hofmann \(2009\)](#); [Hofmann \(2013\)](#) and to induce a lowering of low- $\ell$  power in TT, see Fig. 1 in appendix A. Their implementation in CMB Boltzmann codes is arduous because of the need to introduce a  $q$ -grid for the Boltzmann hierarchy of perturbations to the photon phase-space distribution and a match of low- $z$  with high- $z$  evolutions. Hoping that groups more experienced with the implementation of Boltzmann codes for massive, relativistic species may be interested in pursuing an  $SU(2)_{\text{CMB}}$  code modification, desirably together with the present authors, we have provided information on the low- $z$  dependence of the screening function  $G$  and the associated modified comoving energy-momentum relation for the photon. We have also discussed which CLASS modules need to be targeted in implementing  $SU(2)_{\text{CMB}}$  modifications, both for the cosmological model [Hahn et al. \(2019\)](#) and the linear perturbations thereof.

If the  $SU(2)_{\text{CMB}}$  modifications of CMB codes proposed in the present paper turn out to yield the lowering of low- $\ell$  power in TT under the assumption of statistical isotropy in projecting onto the  $C_\ell$ 's, this would motivate a dedicated analysis of statistical isotropy breaking in terms of less inclusive statistics as a next step. Also, as discussed in Sec. 2.2, a modelling of the depercolation transition from dark energy to dark matter, using the framework of fuzzy dark matter from ultralight axions, would refine Eq. (15) and yield insights in nonlinear structure formation on small scales [Miyatake et al. \(2021\)](#).

## 5 DATA AVAILABILITY

The *Mathematica* notebooks for the computation of the screening function  $G$  and the coefficient  $q/\epsilon$  as well as the modified CLASS code of [Hahn et al. \(2019\)](#) are available from the authors upon request.

## 6 ACKNOWLEDGEMENTS

JM's work is supported by the Vector Foundation under grant number P2021-0102. The authors would like to acknowledge useful discussions with Daniel Kramer and Philip Matthias.

## REFERENCES

- Abbott T. M. C., et al., 2022, *Phys. Rev. D*, 105, 023520  
 Abdalla E., et al., 2022, in 2022 Snowmass Summer Study. ([arXiv:2203.06142](#))  
 Ade P. A. R., et al., 2016, *Astron. Astrophys.*, 594, A13  
 Adler S. L., 1969, *Phys. Rev.*, 177, 2426  
 Adler S. L., Bardeen W. A., 1969, *Phys. Rev.*, 182, 1517  
 Aghanim N., et al., 2016, *Astron. Astrophys.*, 594, A11  
 Aghanim N., et al., 2020, *Astron. Astrophys.*, 641, A6  
 Akrami Y., et al., 2020, *Astron. Astrophys.*, 641, A7  
 Alam S., et al., 2017, *Mon. Not. Roy. Astron. Soc.*, 470, 2617  
 Aluri P. K., Jain P., 2012, *Mon. Not. Roy. Astron. Soc.*, 419, 3378  
 Becker R. H., et al., 2001, *The Astronomical Journal*, 122, 2850–2857  
 Bell J., Jackiw R., 1969, *Nuovo Cim. A*, 60, 47  
 Bennett C. L., et al., 2003, *Astrophys. J. Suppl.*, 148, 1  
 Blas D., Lesgourgues J., Tram T., 2011, *JCAP*, 07, 034  
 Copi C. J., Huterer D., Schwarz D. J., Starkman G. D., 2006, *Mon. Not. Roy. Astron. Soc.*, 367, 79  
 Copi C., Huterer D., Schwarz D., Starkman G., 2007, *Phys. Rev. D*, 75, 023507  
 Copi C. J., Huterer D., Schwarz D. J., Starkman G. D., 2011, *Mon. Not. Roy. Astron. Soc.*, 418, 505  
 Copi C. J., Huterer D., Schwarz D. J., Starkman G. D., 2015a, *Mon. Not. Roy. Astron. Soc.*, 449, 3458  
 Copi C. J., Huterer D., Schwarz D. J., Starkman G. D., 2015b, *Mon. Not. Roy. Astron. Soc.*, 451, 2978  
 Cruz M., Martinez-Gonzalez E., Vielva P., 2010, *Astrophys. Space Sci. Proc.*, p. 275  
 Doran M., 2005, *Journal of Cosmology and Astroparticle Physics*, 2005, 011  
 Eriksen H. K., Hansen F. K., Banday A. J., Gorski K. M., Lilje P. B., 2004, *Astrophys. J.*, 605, 14  
 Falquez C., Hofmann R., Baumbach T., 2010, *Annalen Phys.*, 522, 904  
 Fixsen D. J., et al., 2011, *Astrophys. J.*, 734, 5  
 Fosalba P., Gaztañaga E., 2021, *Monthly Notices of the Royal Astronomical Society*, 504, 5840  
 Fujikawa K., 1979, *Phys. Rev. Lett.*, 42, 1195  
 Fujikawa K., 1980, *Phys. Rev. D*, 21, 2848  
 Giacosa F., Hofmann R., Neubert M., 2008, *JHEP*, 02, 077  
 Gordon C., Hu W., Huterer D., Crawford T. M., 2005, *Phys. Rev. D*, 72, 103002  
 Gruppiso A., Kitazawa N., Lattanzi M., Mandolesi N., Natoli P., Sagnotti A., 2018, *Phys. Dark Univ.*, 20, 49  
 Hahn S., Hofmann R., 2017, *Mon. Not. Roy. Astron. Soc.*, 469, 1233  
 Hahn S., Hofmann R., 2018, *Mod. Phys. Lett. A*, 2016, 1850029  
 Hahn S., Hofmann R., Kramer D., 2019, *Mon. Not. Roy. Astron. Soc.*, 482, 4290  
 Heymans C., et al., 2021, *Astron. Astrophys.*, 646, A140  
 Hinshaw G., Banday A. J., Bennett C. L., Gorski K. M., Kogut A., Lineweaver C. H., Smoot G. F., Wright E. L., 1996, *Astrophys. J. Lett.*, 464, L25  
 Hofmann R., 2007, in 8th Workshop on Quantum Field Theory Under the Influence of External Conditions (QFEXT07). ([arXiv:0710.1169](#))  
 Hofmann R., 2009, *Annalen Phys.*, 18, 634  
 Hofmann R., 2013, *Nature Phys.*, 9, 686  
 Hofmann R., 2015, *Annalen Phys.*, 527, 254  
 Hofmann R., 2016, *The thermodynamics of quantum Yang-Mills theory: Theory and applications*, 2nd edition, World Scientific. World Scientific Publishing Co Pte Ltd  
 Hofmann R., 2018, *AIP Conf. Proc.*, 1978, 300006  
 Hofmann R., Grandou T., 2022, *Universe*, 8, 117  
 Ji S. U., Sin S. J., 1994, *Phys. Rev. D*, 50, 3655  
 Johnson S. D., et al., 2019, *The Astrophysical Journal*, 884, L31  
 Kim J., Naselsky P., 2010, *Astrophys. J. Lett.*, 714, L265  
 Kirkman D., Tytler D., Suzuki N., O'Meara J. M., Lubin D., 2003, *Astrophys. J. Suppl.*, 149, 1  
 Lesgourgues J., 2011, *The Cosmic Linear Anisotropy Solving System (CLASS) I: Overview* ([arXiv:1104.2932](#))  
 Lesgourgues J., Tram T., 2011, *JCAP*, 09, 032  
 Lewis A., Challinor A., Lasenby A., 2000, *The Astrophysical Journal*, 538, 473  
 Ludescher J., Hofmann R., 2009, *CMB dipole revisited*



- ([arXiv:0902.3898](https://arxiv.org/abs/0902.3898))  
 Ma C.-P., Bertschinger E., 1995, *The Astrophysical Journal*, 455, 7  
 Mather J. C., et al., 1990, *Astrophys. J. Lett.*, 354, L37  
 Matos T., Guzman F. S., 2000, *Class. Quant. Grav.*, 17, L9  
 Meinert J., Hofmann R., 2021, *Universe*, 7, 198  
 Miyatake H., et al., 2020, Cosmological inference from emulator based halo model I: Validation tests with HSC and SDSS mock catalogs ([arXiv:2101.00113](https://arxiv.org/abs/2101.00113))  
 Miyatake H., et al., 2021, Cosmological inference from the emulator based halo model II: Joint analysis of galaxy-galaxy weak lensing and galaxy clustering from HSC-Y1 and SDSS ([arXiv:2111.02419](https://arxiv.org/abs/2111.02419))  
 Niemeyer J. C., 2020, *Progress in Particle and Nuclear Physics*, 113, 103787  
 Notari A., Quartin M., 2015, *JCAP*, 06, 047  
 Nunes R. C., Vagnozzi S., 2021, *Monthly Notices of the Royal Astronomical Society*, 505, 5427  
 Perlmutter S., et al., 1999, *Astrophys. J.*, 517, 565  
 Riess A. G., et al., 1998, *Astron. J.*, 116, 1009  
 Riess A. G., et al., 2021, A Comprehensive Measurement of the Local Value of the Hubble Constant with 1 km/s/Mpc Uncertainty from the Hubble Space Telescope and the SH0ES Team ([arXiv:2112.04510](https://arxiv.org/abs/2112.04510))  
 Shive H.-Y., Chiueh T., Broadhurst T., 2014, *Nature Phys.*, 10, 496  
 Schwarz M., Hofmann R., Giacosa F., 2007a, *JHEP*, 02, 091  
 Schwarz M., Hofmann R., Giacosa F., 2007b, *Int. J. Mod. Phys. A*, 22, 1213  
 Schwarz D. J., Copi C. J., Huterer D., Starkman G. D., 2016, *Class. Quant. Grav.*, 33, 184001  
 Seljak U., Zaldarriaga M., 1996, *The Astrophysical Journal*, 469, 437  
 Shull J. M., Smith B. D., Danforth C. W., 2012, *Astrophys. J.*, 759, 23  
 Sin S.-J., 1994, *Phys. Rev. D*, 50, 3650  
 Sugiyama S., et al., 2021, HSC Year 1 cosmology results with the minimal bias method: HSC×BOSS galaxy-galaxy weak lensing and BOSS galaxy clustering ([arXiv:2111.10966](https://arxiv.org/abs/2111.10966))  
 Szopa M., Hofmann R., 2008, *JCAP*, 03, 001  
 Tegmark M., de Oliveira-Costa A., Hamilton A., 2003, *Phys. Rev. D*, 68, 123523  
 Vielva P., 2010, *Adv. Astron.*, 2010, 592094  
 Vielva P., Martinez-Gonzalez E., Barreiro R. B., Sanz J. L., Cayon L., 2004, *Astrophys. J.*, 609, 22  
 Wong K. C., et al., 2020, *Mon. Not. Roy. Astron. Soc.*, 498, 1420  
 Yeung S., Chu M.-C., 2022, *Physical Review D*, 105  
 de Oliveira-Costa A., Tegmark M., Zaldarriaga M., Hamilton A., 2004, *Phys. Rev. D*, 69, 063516

## APPENDIX A: $SU(2)_{\text{CMB}}$ CMB FIT

A lowering of the  $TT$  power spectrum for small  $\ell$  is expected Hofmann (2013) when taking screening / antiscreening effects into account in the comoving dispersion law of the low- $z$  photon, see Eq. (26) and Fig. 5. This may close the red shaded area in Fig. 1 below. Beyond such a lowering of small- $\ell$   $TT$  power, the investigation of statistical-isotropy breaking, induced by a cosmologically local temperature depression and characterised by a typical gradient Gordon et al. (2005); Hofmann (2013), requires less inclusive statistics, see e.g. Schwarz et al. (2016).

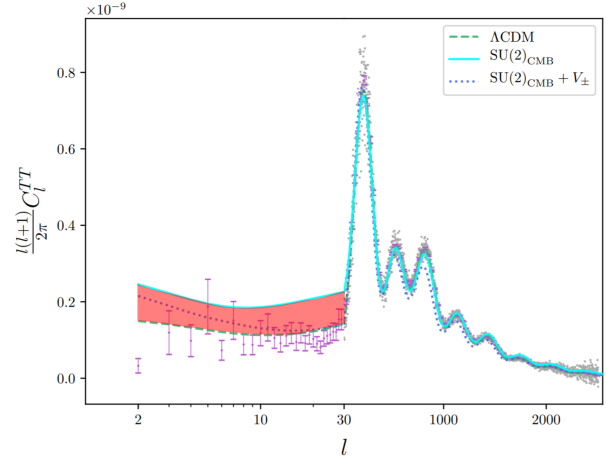


Figure 1: Normalised power spectra of  $TT$  correlator for best-fit parameter values quoted in Table 1. Figure adapted from Hahn et al. (2019).